MATERIALS CHARACTERIZATION 59 (2008) 79–83

Microstructure and texture of duplex stainless steel after melt-spinning processing

C. Herrera[a,*], N.B. de Lima[b], A.M. Kliauga[a], A.F. Padilha[a]

[a]Department of Metallurgical and Materials Engineering, University of São Paulo, Av. Prof. Mello Moraes 2463, CEP — 05508-900 S. Paulo, Brazil

[b]Instituto de Pesquisas Energéticas e Nucleares, CCTM, Av. Prof. Lineu Prestes, 2242, CEP 05508-900, S. Paulo, Brazil

ARTICLE DATA

Article history:
Received 16 September 2006
Accepted 30 October 2006

Keywords:
Melt spinning
Duplex stainless steel
Microstructure
Texture

ABSTRACT

The microstructure and texture of melt-spun UNS S31803 (DIN W. Nr. 1. 4462) duplex stainless steel were analyzed after casting and solution treatment. The cast ribbons contained austenite (γ) and ferrite (α or δ) with roughly equal compositions. The α and γ had <100> and <110> partial fiber textures, respectively. After solution treatment, the texture was maintained, the amount of γ phase increased, and the alloying elements were partitioned as expected, according to whether they were ferrite or austenite stabilizers.

1. Introduction

Published research on rapid solidification of two phase alloys having a duplex microstructure, and especially for duplex steels is limited. The study of rapid solidification is relevant to the production, as well as to the welding, of these materials. The use of melt spinning as an investigative tool permits good control of the cooling rates, and provides the opportunity to control and understand the crystallographic texture of these duplex stainless steels; this understanding is important to their optimization.

Duplex stainless steels present a better combination of mechanical properties and corrosion resistance than single-phased ferritic and austenitic stainless steels. They are based on the Fe–Cr–Ni system and generally contain two phases in approximately equal volume fractions: ferrite (α or δ) and austenite (γ). In addition to Fe, Cr and Ni, they contain other chemical elements that are classified as either ferrite (Cr, Mo, Si) or austenite (Ni, N, C, Mn, Cu) stabilizers. The efficiency of these elements as ferrite and austenite stabilizers can be expressed by their Cr and Ni (equivalency). Among several equations for Cr_{eq} and Ni_{eq}, one can consider the following [1]:

$$Cr_{eq} = Cr + 1.37Mo + 1.5Si + 2Nb + 3Ti \quad (1)$$

$$Ni_{eq} = Ni + 0.3Mn + 22C + 14.2N + Cu \quad (2)$$

By using Cr_{eq} and Ni_{eq}, it is possible to predict the solidification sequence or mode [2]:

a) Cr_{eq}/Ni_{eq} = 1.38–1.5: L→L+γ→L+γ+δ→γ+δ (mode Austenitic–Ferritic — AF)
b) Cr_{eq}/Ni_{eq} = 1.5–2.0: L→L+δ→L+δ+γ→δ+γ (mode Ferritic–Austenitic — FA)
c) Cr_{eq}/Ni_{eq} > 2.0: L→L+δ→δ (mode Ferritic — F)

Duplex stainless steel may solidify in modes FA or F. The FA mode means that austenite forms either from the liquid or, for the F mode, in the solid state during cooling. The amount of austenite formed and its morphology are very sensitive to the

* *Corresponding author*. Tel.: +55 11 40709626.
E-mail address: cherrera@usp.br (C. Herrera).

1044-5803/$ – see front matter © 2006 Elsevier Inc. All rights reserved.
doi:10.1016/j.matchar.2006.10.022

cooling rate [3–5]. Cvjović et al. [6] have studied the solidification in welds of a duplex stainless steel with $(Cr/Ni)_{eq}=1.8$ (solidification mode FA) at various cooling rates. For cooling rates varying from 10 to 10^3 K/s and low undercooling (1.5 to 1.3 K), they concluded that the solidification mode was unchanged, but the microstructural morphology changed from thick to thin intercellular γ and the volume fraction of ferrite δ increased. For a cooling rate of 10^4 K/s and undercooling greater than 75 K, the solidification mode changed to F and a δ grain structure with intragranular γ Widmanstätten morphology was observed [6].

Melt spinning is a rapid solidification method presenting cooling rates between 10^3 and 10^9 K/s [7,8]. It involves many variables that determine the microstructure and properties of the resulting steel tape. Steel tapes produced by melt spinning consist of columnar grains growing from the chilling zone, which is the spinning wheel surface (WS). Melt-spun ribbons exhibit a strong <100> fiber texture, rotated from about 20° in relation to the normal ribbon [9,10]. The aim of this work is to characterize the microstructure and texture of DIN 1.4462 (UNS S31803) duplex stainless steel ribbons produced by melt spinning, after casting and after solution treatment.

2. Experimental Procedure

Rapidly solidified ribbons of DIN 1.4462 (UNS S31803), approximately 0.05 mm thick, were produced in an argon atmosphere by single roller melt spinning. The base material was first heated by an induction coil to melting in a quartz crucible and then ejected by a 90 kPa helium flux onto a copper wheel rotating at 25 m/s. The quartz crucible had an outlet orifice of 1.5 mm. The alloy composition is shown in Table 1. After casting, samples were solution treated at 1373 K for 1 h in a 100 kPa argon atmosphere and quenched in water.

The microstructure of the samples was observed with optical (OM), scanning electron (SEM) and transmission electron (TEM) microscopes. A chemical analysis was performed by an energy dispersion spectroscopy (EDS) device attached to the SEM. Microhardness measurements were taken using a load of 0.025 kg.

X-ray diffraction analysis was performed with CuKα (1.54056 Å) radiation at the wheel surface (WS) and at the free surface (FS) of the as cast and the solution treated samples. This technique was used to identify and to quantify the phases present in each state. Austenite (γ) and ferrite (α) volume fractions were obtained by the direct comparison method given by Cullity [11]. The texture of the samples was analyzed by an automated texture goniometer attached to a Rigaku diffractometer using MoKα (0.7093 Å) radiation. Pole figures were obtained for the (200), (211) and (321) planes in austenite, for the (220), (200) and (311) planes in ferrite and for both surfaces (WS and FS).

3. Results and Discussion

The DIN 1.4462 steel had a Cr_{eq}/Ni_{eq} of 3.14 and thus, according to the El Nayal and Beech criterion [2] solidified in the F mode with austenite forming in the solid state during cooling.

The cast ribbon was characterized in the longitudinal cross section, at the wheel surface (WS), Fig. 1A, and at the free surfaces (FS). When the samples were observed along the longitudinal cross section (Fig. 1B), a columnar grain ferrite was rotated approximately 15° in relation to the WS normal, and Widmanstätten austenite needles were seen at the grain boundaries, Fig. 1C. At the WS, the microstructure was composed of equiaxed ferrite grains, and the grain size distribution was not homogeneous but varied from region to region, characterized by grains of 3 μm diameter and larger. At the FS, the grains were also equiaxed but larger than at the WS. Austenite needles, formed during cooling, were also observed by TEM inside the ferrite grains, Fig. 1C.

After solution heat treatment (Fig. 2) the equiaxed morphology was lost, since ferrite was partially consumed by austenite formation, Fig. 2A. In the longitudinal cross section, Fig. 2B, the grains maintained a bent columnar microstructure, but the reduction of the ferrite volume fraction was evident, from approximately 72% to 39%, Table 2.

Table 2 presents the cell parameter, volume fraction and microhardness of the austenite and ferrite phases in the cast ribbon and after solution treatment at 1373 K. Despite the differences in composition, the cell parameter and the hardness of the two phases in the ribbon and after solution treatment did not vary much in relation to the theoretical International Centre for Diffraction Data (ICDD) values for austenite and ferrite [12,13] and to published data for conventionally-produced duplex stainless steel [14–16]. This is because the main substitutional atoms (Cr, Ni, Mn) have atomic radii close to that of iron and they do not produce significant cell distortion in austenite or ferrite [17]. The ferrite phase lattice parameter did not change significantly with the heat treatment, while the austenite phase lattice parameter showed a small decrease. A relationship between austenite volume fraction and the lattice parameter was presented by Ribeiro Miranda et al. [16]; those results agree with those given in this paper.

The Energy Dispersion Spectroscopy of Fe, Cr, Ni, Mo, Mn and Si in austenite and ferrite were interpreted as a function of the partition coefficient K_i:

$$K_i = \frac{X_i^{\alpha}}{X_i^{\gamma}} \tag{3}$$

where X_i^{α} and X_i^{γ} represent the concentration of element i in phases α and γ, respectively, Fig. 3.

In the cast ribbon, the austenite and ferrite concentrations were very similar, probably due to the fast cooling rate, which

Table 1 – Chemical composition of the studied DIN 1.4462 steel (wt.%)

C	Cr	Ni	N	Mo	W	S	Mn	Nb	Si	P	Ti	V
0.025	22.04	5.49	0.14	2.91	0.03	0.01	1.72	0.013	0.47	0.021	0.01	0.11

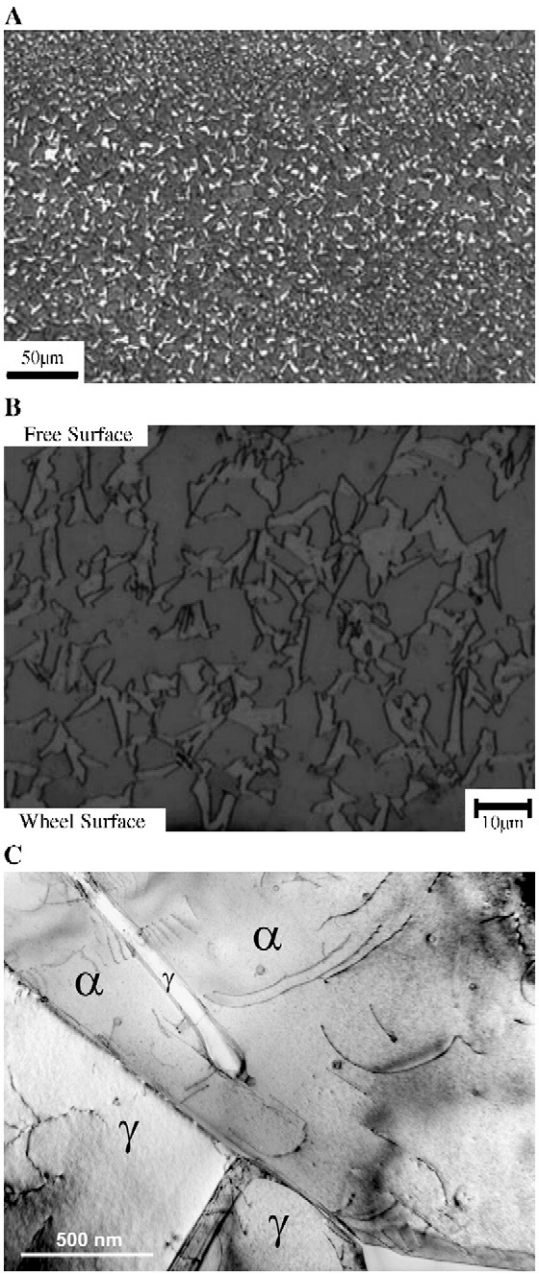

Fig. 1 – Optical micrograph for the ribbon: (A) on the wheel surface side; (B) in a longitudinal cross section; (C) austenite needles precipitated inside a ferrite grain (TEM).

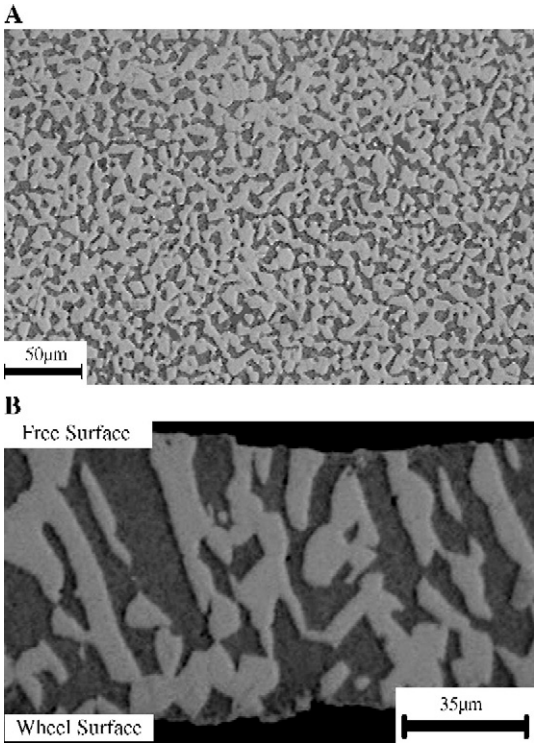

Fig. 2 – Optical micrograph for the ribbon after solution annealing at 1373 K: (A) free surface; (B) longitudinal cross section.

significantly reduces the time available for diffusion. After the solution treatment, the ferrite was enriched in Cr, Mo and Si, whereas the austenite was enriched in Ni, Mn and Fe. This elemental partitioning coincided with the stabilizing effect of each analyzed element, and is consistent with the results from the literature [18,19].

The (200) pole figure for the ferrite, and the (220) pole figure for the austenite on the WS in the as-cast condition are shown in Fig. 4 A and B, respectively. The (100) ferrite planes are parallel to the (110) austenite planes and both are rotated 15° in relation to normally-cast ribbon. The interpretation of the group of measured pole figures indicates that the ferrite presented a <100> fiber texture which was weaker on the WS (times random, TR=9.5) than on the FS (TR=11.7). All these features are common for columnar solidification in cubic metals and coincide with the rotation of the columnar grains observed by metallography. The X-ray penetration was less than 16 μm and the lower intensity at the WS may be an indication that random cellular solidification occurred on this surface. As columnar growth initiated, the <100> fiber texture increased in the FS direction. This rotation was due to the thermal gradient experienced in the melt-spinning process [9,10,20]. The austenite was formed during cooling from the ferrite grain boundaries and presented a partial <100> fiber texture, which had a stronger (110)[11¯2] component at the WS (TR=4.21) changing to a (110)[11¯1] component at the FS (TR=4.49).

Table 2 – Cell parameter, volume fraction and microhardness of austenite and ferrite in the cast ribbon and after solution annealing at 1373 K

	Phase	Calculated cell parameters, nm	Volume fraction wt.%	Microhardness, HV
Cast ribbon	Ferrite	0.2876	72.2	252±10
	Austenite	0.3616	27.8	266±8
Solution heat treated at 1373 K	Ferrite	0.2878	38.7	251±16
	Austenite	0.3607	61.3	259±12

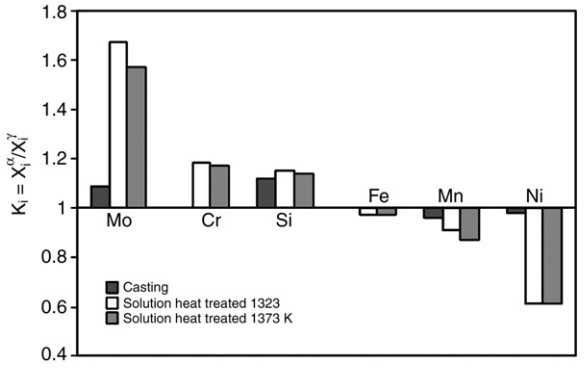

Fig. 3 – Partition coefficient $K_i = X_i^{\alpha} / X_i^{\gamma}$ of the alloying elements in the as-cast and heat treated ribbons.

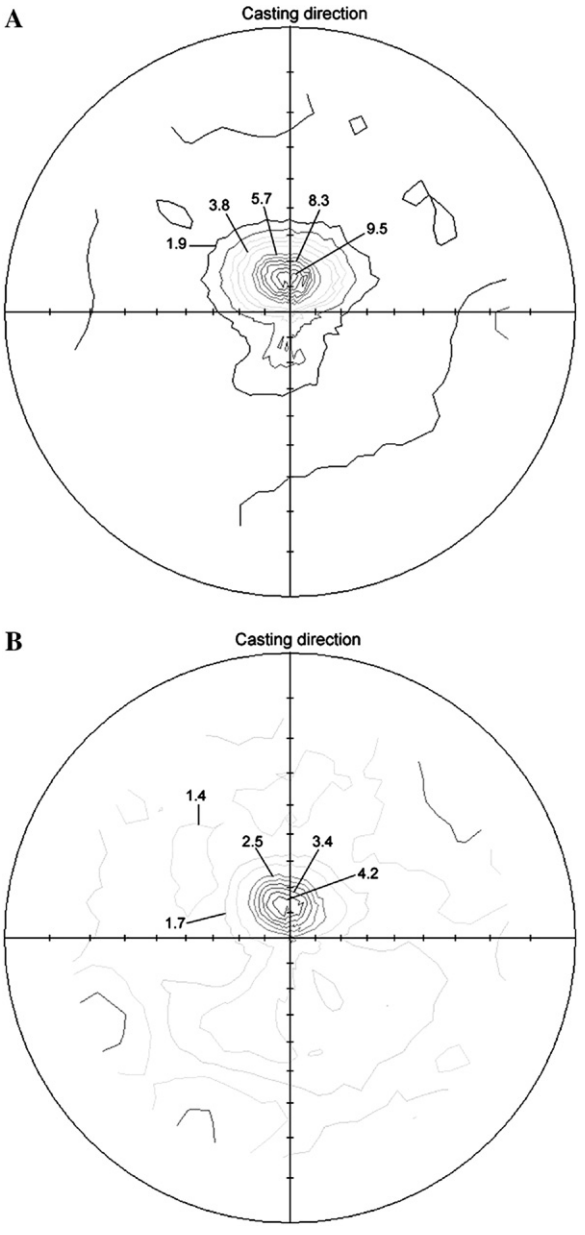

Fig. 4 – Cast ribbons on the wheel surface (WS): A) (200) pole figure for the ferrite and; B) (220) pole figure for the austenite.

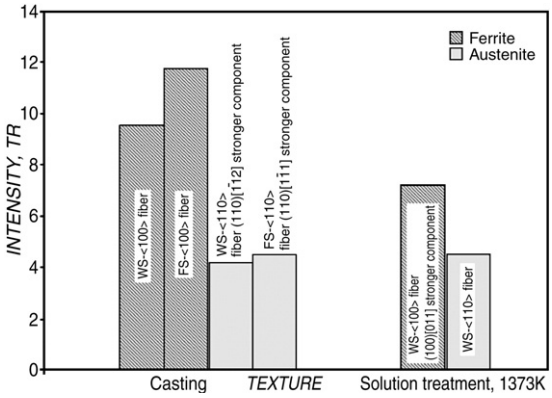

Fig. 5 – Texture intensities at the WS and the FS for the different main orientations in austenite and ferrite in the as cast, and the solution annealed (1373 K) ribbon.

After solution treatment, there was a change at the WS: the ferrite <100> fiber texture diminished to ease the formation of the (100)[011] component (TR = 7.21), and the austenite <100> fiber texture increased, probably due to the increase of the γ volume fraction. Both phases maintained the 15° rotation to the normal ribbon on both surfaces. Fig. 5 summarizes the texture results, showing the main texture components and their intensities in the ferrite and austenite, in the as-cast condition and after solution annealing.

4. Conclusions

The ribbon solidified in a ferritic mode, presenting a higher volume fraction of ferrite than would be formed in the solid state. The microstructure and the texture changed across the ribbon thickness. At the wheel surface, due to rapid solidification, the ferrite solidified with a very fine, equiaxed morphology. When leaving the wheel surface, the grains turned into a more columnar morphology and the grains were thicker at the free surface.

The ferrite presented a <100> fiber texture, which is typical for rapid solidified cubic metals. The austenite presented a partial <100> fiber texture. The texture of both phases had a higher intensity on the free surface and was rotated 15° from the normal wheel surface.

After solution annealing at 1373 K, the amount of austenite increased, the microstructure was characterized by columnar ferrite grains in the longitudinal cross section, losing their equiaxed morphology at both the free (FS) and wheel (WS) surfaces. The texture at the wheel surface changed — the ferrite <100> fiber texture weakened and a (100)[011] component was formed. In the austenite, the <100> fiber texture increased, probably due to a higher γ volume fraction.

The partition of the ferrite and austenite stabilizing elements after casting did not follow normal ferrite or austenite formation characteristics. This was probably due to the rapid cooling rate during melt spinning. After solution annealing the alloying elements were found to be partitioned according to their characteristic preference as austenite or ferrite formers.

Acknowledgments

The authors are grateful to CAPES, CNPq and FAPESP (Brazil) for the financial support of this work. Thanks are also due to Dr. Ronald Lesley Plaut (University of S. Paulo, Brazil) for going through the manuscript meticulously.

REFERENCES

[1] Suutala N, Moisio T. Solidification and casting of metals. London: Metals Society; 1979. p. 310.
[2] El Nayal G, Beech J. Relationship between composition, impurity content, cooling rate and solidification in austenitic stainless steel. Mat Sci Technol 1986;2:603–10.
[3] Johnson E, Gråbæk L, Johansen A, Sarholt Kristensen L. Microstructure of rapidly solidified stainless steel. Mater Sci Eng 1988;98:301–3.
[4] Viteck JM, Dasgupta A, David SA. Microstructural modification of austenitic stainless steel by rapid solidification. Metall Trans A 1983;14:1833–41.
[5] David SA, Viteck JM, Hebble TL. Effect of rapid solidification on stainless steel weld metal. Microstructures and its implications on the Schaeffler diagram. Welding Research Sup Oct 1987:289S–300S.
[6] Cvijović ZM, Mihajlović DV, Knežević VR. Microstructural morphology and stability of rapidly solidified duplex stainless steel. Mat Sci Forum 1998;282–283:323–30.
[7] Anatharaman TR, Suryanarayana C. Rapidly solidified metals: a technological overview. Brookfield: E.U.A: Trans Tech Publications; 1987.
[8] Martin JW, Doherty RD, Cantor B. Stability of microstructure in metallic systems. 2nd ed. Cambridge, NY: Cambridge University Press; 1997. p. 426.
[9] Wakamiya M, Horita Y, Senno H, Hirota E. In: Masumoto T, Suzuki K, editors. Rapidly quenched metals, vol. II. The Japan Institute of Metals: Sendai; 1982. p. 1577–80.
[10] Tenwick MJ, Davies HA. Int. The structure and properties of rapidly solidified Fe – 3 to 9.3 wt.% Si alloys. J. Rapidly Sol. 1984-85; 1: 143–155.
[11] Cullity BD. Elements of X-ray diffraction. Upper Saddle River. 3rd ed. NJ: Prentice Hall; 2001. p. 402–33.
[12] IDCC — International Center for Diffraction Data. Card Nr. 06–0696. 1995.
[13] IDCC — International Center for Diffraction Data. Card Nr. 31–0619. 1995.
[14] Nilsson JO. Superduplex stainless steel. Mater Sci Technol 1992;8:685–700.
[15] Padilha AF, Randle V, Machado IF. Microstructure and microtexture changes during solution nitriding to produce austenitic case on ferritic–austenitic duplex stainless steel. Mater Sci Technol 1999;15:1015–8.
[16] Ribeiro Miranda MA, Sasaki JM, Tavares SSM, de Abreu HFG, Neto JM. The use of X-ray diffraction, microscopy, and magnetic measurements for analysing microstructural features of a duplex stainless steel. Mater Charact 2005;54:387–93.
[17] Lee YK, Hong J, Choi CS, Lee JK. Continuous cooling transformation temperatures and microstructures of niobium bearing microalloyed steels. Mat Sci Forum 2005;475–479:65–8.
[18] Atamert S, King JE. Sigma phase formation and its prevention in duplex stainless steel. J Mat Sci Lett 1993;12:1144–7.
[19] Chen TH, Yang JR. Effects of solution treatment and continuous cooling σ-phase precipitation in a 2205 duplex stainless steel. Mater Sci Eng A 2001;311:28–41.
[20] Huang SC, Laforce RP, Ritter AM, Goehner RP. Rapid solidification characteristics in melt spinning a Ni-base superalloy. Metall Trans A 1985;16A:1773–9.